PHYSICAL REVIEW B, VOLUME 64, 205410

Inelastic scattering of fast electrons in nanowires: A dielectric formalism approach

N. Zabala,[1,2] E. Ogando,[1] A. Rivacoba,[2,3] and F. J. García de Abajo[2]
[1]*Elektrika eta Elektronika Saila, Zientzi Fakultatea, UPV/EHU, 644 P.K., 48080 Bilbo, Spain*
[2]*Donostia International Physics Center (DIPC) and Centro Mixto CSIC-UPV/EHU, Aptdo. 1072, 20080 San Sebastian, Spain*
[3]*Materialen Fisika Saila, Kimika Fakultatea, UPV/EHU, 1072 P.K., 20080 Donostia, Spain*
(Received 25 April 2001; published 31 October 2001)

The excitations produced by fast electrons impinging perpendicularly on both metallic and semiconductor cylindrical nanowires are investigated within the framework of dielectric theory. The dependence of the electron energy-loss spectra (EELS) on the nanowire radius is studied in detail, and so is the spatial extension of the induced-charge fluctuations associated to the modes that are excited during the loss process. The limits of applicability of dielectric theory to nanowires are discussed. In particular, comparison between the present theory and EELS measurements performed with silicon nanofibers support the use of dielectric theory at the scale of a few nanometers in diameter, and it is shown that this positive result is justified in terms of the longitudinal pattern of the induced surface plasmons. Finally, the effect of nanowire termination on the electron energy-loss probability for electrons passing near the edge is calculated using the boundary charge method, showing that the range of this effect can extend up to tens of nanometers for low-energy $m=0$ modes.

DOI: 10.1103/PhysRevB.64.205410 PACS number(s): 71.45.Gm, 68.49.Uv, 79.20.−m

I. INTRODUCTION

Technical developments in nanofabrication have allowed in recent years the production of structures of nanometric size with different shapes and compositions. This has stimulated considerable theoretical and experimental work leading to a better general understanding of these nanostructures and the relevant physics at this length scale. While some of these structures are very promising candidates for applications in nanoscale electronic devices, wires or nanotubes of a few nanometers in radius and some tens or hundreds of micrometers in length are particularly interesting from a fundamental point of view due to their quasi-one-dimensional character. In this context, the availability of tubular fullerenes has opened a field of research in nanophysics,[1,2] and great progress is being made in obtaining solid nanowires and even nanowires encapsulated in nanotubes.[3,4] Multielement nanotubes have been recently synthesized by means of reactive laser ablation, reproducing coaxial nanocables intercalating semiconductor and metallic materials.[5] Among the commonly employed experimental tools, many studies have relied on transmission-electron microscopy (TEM) to image these nanostructures and electron energy-loss spectroscopy (EELS) to study their response. The high-energy losses associated with core excitations is more often used to characterize the chemical composition of the sample, where spatially resolved EELS, using finely focused 100-keV electron probes, have allowed analysis of atomic concentrations of single[6] and multiwall[7,8] carbon nanotubes as well as elemental profiles across synthesized complex nanotubes[9] and nanocables.[5] On the other hand, valence loss spectroscopy provides information about plasmon excitations and interband transitions, at the cost of a higher degree of delocalization owing to the fact that plasmons are supported by extended charge fluctuations. It is in this latter case where the analysis of the spectra relies more on theories such as the one developed in this work.

To the best of our knowledge, the first theoretical works on plasmon excitations in cylindrical interfaces appeared in the early 1970s, motivated by light reflection experiments[10,11] and studies of losses in particle accelerators.[12] After that, the interest in the cylindrical geometry increased in the 1980s due to the ability shown by the scanning TEM (STEM) electron beam to drill holes and lines of nanometer size in some inorganic materials. In order to explain those experiments, expressions for the energy loss in clean and metal-coated holes have been reported for trajectories parallel to the axis of the cylinder.[13–15] Also, collective excitations in carbon nanotubes have been the subject of study in different theoretical papers in recent years.[16–18] A general expression of the energy-loss probability valid for any beam direction, including trajectories penetrating the cylinder, was obtained by Rivacoba *et al.*[19] in the framework of dielectric theory. This study has been extended to consider tubular fullerenes by Bertsch *et al.*[20] by assuming a nonisotropic response of the medium, as proposed by Lucas and coworkers.[21] The self-energy formalism has been also applied to the case of a cylinder interacting with a broad beam.[22]

Recently, Reed *et al.*[23] have reported a detailed EELS characterization of single-crystal silicon tips and filaments, finding quite good qualitative agreement with the spectra obtained from the dielectric theory for diameters down to 3.5 nm. Nevertheless, the suitability of dielectric theory for such small targets is questionable. As a matter of fact, there is contradictory experimental evidence in the literature. On the one hand, Ouyang *et al.*[24] reported fine EELS measurements of Ag hemispheres and a thorough study of these results[25] showed that dielectric theory reproduces reasonably well the experiments for hemispheres of radii larger than 4 nm, but it breaks down for smaller targets. On the other hand, Fehlhaber and Bursill have recently proved that in small spherical diamond particles of about 3 nm in radius, both with clean surfaces[26] or covered with amorphous carbon,[27] the dielectric theory leads to good agreement with the experimental energy-loss spectra. Measurements of the optical response of

Li (Ref. 28) and Na (Ref. 29) clusters have also shown that the macroscopic dielectric function is a pertinent parameter to interpret cluster data for clusters containing up to about 100 atoms. This seems to indicate that dielectric theory is suitable in cases where it is fair to consider the valence electronic structure as a continuum, and therefore, its validity depends not only on the size of the target, but also on the electronic structure of the medium. An intuitive and simple explanation for the mentioned discrepancy with respect to the range of applicability of dielectric theory between silver and diamond targets is given by the difference in energy of plasmon excitations in these nanostructures: ~ 3.5 eV for silver versus ~ 20 eV for diamond; the larger the excitation energy, the less sensitive the response to details in the electronic structure, and therefore, the more justified the continuum approach underlying the dielectric theory.

Apart from the electronic character of the material, long wires are substantially different from small finite systems: electrons in wires are confined in the transverse direction but free to move in the longitudinal one (i.e., it is an open system) and consequently their associated electronic structure is continuous in the longitudinal direction and can be discrete in the transverse one.[30,31] This fact suggests that the dielectric theory for such targets is likely to be valid for excitations corresponding to longitudinal charge-density fluctuations. In this sense it is useful to point out that the surface-plasmon dispersion relation can be labeled $\omega_m = \omega_m(q)$, where m is the azimuthal number and q is the longitudinal component of the momentum.[32,33,19] This form of the dispersion relation indicates that there are contributions from a continuum of longitudinal wave vectors in the energy-loss spectra, and therefore, the validity of the dielectric theory in small wires should depend on the relative strength of contributions coming from low momentum q and from low azimuthal number m.

The aim of this paper is to establish the limits of applicability of dielectric theory in the study of inelastic scattering of fast electrons by thin wires. Following Ref. 19, theory and experiment are contrasted by considering a situation where an electron beam impinges on a long cylinder describing a penetrating trajectory normal to the axis of the wire. The emphasis is placed on the contribution to the energy-loss spectra coming from different quantum numbers q and m, associated with different plasmon excitations. Moreover, the analytical properties of the so-called ''begrenzungseffekt'' (i.e., the surface correction to the bulk-plasmon excitation probability) are analyzed, and the radius dependence of the loss probability for a metallic target is discussed as well (Sec. II). The case of silicon nanowires is considered in Sec. III, finding excellent agreement with the experimental results of Ref. 23. This agreement is explained in terms of the predominance of longitudinal excitations in the EELS spectrum (i.e., small q's). In Sec. IV, the boundary charge method[34] (BCM) is applied to study the effect of the finite size of the wire on the EELS spectra. The energy of the $m=0$ loss peak in Si wires is found to be independent of the position of the beam relative to the wire edge, while its intensity is sensitive to that parameter beyond the range of the ω component of the potential induced by the probe. Using a retarded version of the BCM,[35] retardation effects have been proven to be irrelevant for the impact parameters and targets under consideration (although they play a relevant role for larger diameters), and therefore, they are completely disregarded.

II. FORMULATION OF EELS IN INFINITE CYLINDERS; PERPENDICULAR TRAJECTORY

We describe the nanowires as infinite cylinders of radius a, characterized by their dielectric response function ϵ and consider the probe electron moving with velocity $\mathbf{v}$ along a straight trajectory (x axis). Atomic units (a.u., that is, $\hbar = e^2 = m = 1$) and the Gaussian unit system will be used throughout this work, unless otherwise specified. The electron-target interaction is described by the self-energy formalism and the energy-loss probability can be expressed in terms of the screened interaction[36] $W(\mathbf{r},\mathbf{r}',\omega)$, neglecting the electron recoil,

$$P(\omega) = \frac{1}{\pi v^2} \int_{-\infty}^{\infty} dx' \int_{-\infty}^{\infty} dx \, \mathrm{Im}\{ W(\mathbf{r},\mathbf{r}',\omega) \times e^{i(\omega/v)(x-x')} \}|_{traject}, \tag{1}$$

where both $\mathbf{r}$ and $\mathbf{r}'$ are evaluated along the trajectory. This equation accounts for the total energy-loss probability, containing both bulk and surface contributions. When describing cylindrical surfaces, it is helpful to write the screened interaction in terms of cylindrical coordinates $\mathbf{r} = (\rho, z, \phi)$ as follows:

$$W(\mathbf{r},\mathbf{r}',\omega) = \frac{2}{\pi} \sum_{m=0}^{\infty} (2-\delta_{m0}) \int_0^{\infty} dq \cos[q(z-z')] \times \cos[m(\phi-\phi')] W_m(q,\rho,\rho',\omega), \tag{2}$$

where q is the momentum along the axis of the cylinder and the m components $W_m(q,\rho,\rho',\omega)$ can be written as an appropriate combination of Bessel functions in the inner and outer parts of the wire. Then, after matching the boundary conditions at the cylindrical interface $\rho = a$, the screened interaction is obtained.[19] Notice that expression (2) is valid for any ω-dependent dielectric function. This fact allows us to use experimental data of the dielectric functions, which have been proven to describe in detail the energy-loss spectra for fast electrons.[37] In this approach, dispersion effects deriving from the momentum dependence of the dielectric function[38–41] are ignored. Nevertheless, local effects in the surface dielectric response are relevant only when high values of the momentum transfer are involved[40] and, as we will see for nanowires, even for penetrating probe trajectories, the values of both q and m which contribute significantly to inelastic scattering are very small, so that the local approach is fully justified.

For trajectories perpendicular to the cylinder axis, the position of the probe at impact parameter s is defined by the Cartesian coordinate x, related to $\rho(x) = (x^2 + s^2)^{1/2}$ and $\phi(x) = \arctan(x/s)$. The geometric parameters have been sketched in the inset of Fig. 5 below, where the circle repre-

sents the cylinder cross section. After some algebra,[19] the surface contribution to the loss probability can be written as

$$P_{surf}(\omega)=\frac{8}{\pi^2 v^2}\sum_{m=0}^{\infty}(2-\delta_{m0})\int_0^{\infty}dq\Bigg\{\mathrm{Im}\left(\frac{1}{\epsilon_1}\right)\times\left[\frac{K_m(qa)}{I_m(qa)}(S_{i(m)}^2+C_{i(m)}^2)+S_{i(m)}S_{o(m)}+C_{i(m)}C_{o(m)}\right]+\mathrm{Im}\left(\frac{1}{\epsilon_2}\right)\left[\frac{I_m(qa)}{K_m(qa)}\times(S_{o(m)}^2+C_{o(m)}^2)+S_{i(m)}S_{o(m)}+C_{i(m)}C_{o(m)}\right]+\mathrm{Im}[\gamma_m(q,\omega)]\left[\frac{K_m(qa)}{I_m(qa)}(S_{i(m)}^2+C_{i(m)}^2)+\frac{I_m(qa)}{K_m(qa)}(S_{o(m)}^2+C_{o(m)}^2)+2(S_{i(m)}S_{o(m)}+C_{i(m)}C_{o(m)})\right]\Bigg\}, \tag{3}$$

where $\mathrm{Im}(x)$ stands for the imaginary part of x, and the cylindrical surface response function $\gamma_m(q,\omega)$ is given by

$$\gamma_m(q,\omega)=\frac{1}{qa[\epsilon_1 I_m'(qa)K_m(qa)-\epsilon_2 I_m(qa)K_m'(qa)]}, \tag{4}$$

where $K_m(x)$ and $I_m(x)$ are the modified Bessel functions, and the prime stands for the derivative with respect to the argument. The coefficients $S_{i,o(m)}$ and $C_{i,o(m)}$ are functions of both q and ω, defined as follows:

$$S_{i(m)}(q,\omega)=\int_0^{x_a}dx\,\sin[m\phi(x)]\sin(\omega x/v)I_m(q\sqrt{x^2+s^2}),$$

$$C_{i(m)}(q,\omega)=\int_0^{x_a}dx\,\cos[m\phi(x)]\cos(\omega x/v)I_m(q\sqrt{x^2+s^2}),$$

$$S_{o(m)}(q,\omega)=\int_{x_a}^{\infty}dx\,\sin[m\phi(x)]\sin(\omega x/v)K_m(q\sqrt{x^2+s^2}),$$

$$C_{o(m)}(q,\omega)=\int_{x_a}^{\infty}dx\,\cos[m\phi(x)]\cos(\omega x/v)K_m(q\sqrt{x^2+s^2}), \tag{5}$$

where $x_a=\sqrt{a^2-s^2}$ for penetrating trajectories ($a>s$), or zero otherwise. Equation (3) provides the surface contribution to the inelastic scattering; to get the total-energy-loss probability, the bulk energy loss experienced by the probe when moving through each medium should be added; this magnitude is proportional to the path length inside each medium. If we assume the simple case of a wire of dielectric function $\epsilon(\omega)$ surrounded by vacuum, then

$$P_{total}(\omega)=P_{surf}(\omega)+\frac{2}{\pi v^2}2x_a\mathrm{Im}\left[\frac{-1}{\epsilon(\omega)}\right]\ln\left[\frac{q_{max}v}{\omega}\right], \tag{6}$$

where q_{max} is a cutoff momentum.[42] For nonpenetrating trajectories ($a<s$), $x_a=0$, both integrals $S_{i(m)}$ and $C_{i(m)}$ are zero, and the integrals $S_{o(m)}$ and $C_{o(m)}$ have been analytically calculated by Bertsch *et al.*[20]

In Eq. (3), the term containing the response function $\gamma_m(q,\omega)$ describes the excitation of surface plasmons, while the first two terms, containing the bulk loss functions $1/\epsilon_{1,2}$, yield a negative correction to the bulk excitation probability experienced by the probe when moving through an infinite medium. This is the so-called *begrenzung* or boundary effect, first found by Ritchie for electrons traversing thin films.[43] The analytical properties of this correction can be better understood if both media are described by two Drude dielectric functions with plasmon frequencies ω_{p1} and ω_{p2}. Then, the imaginary part of the surface response function can be written as

$$\mathrm{Im}[\gamma_m(q,\omega)]=\frac{\pi}{2}\omega_m(q)[(\omega-\omega_m(q)], \tag{7}$$

where the energy of the surface plasmon $\omega_m(q)$ is then given by the dispersion relation

$$\omega_m(q)^2=qa[I_m'(qa)K_m(qa)\omega_{p1}^2-I_m(qa)K_m'(qa)\omega_{p2}^2]. \tag{8}$$

Taking into account that now the loss functions are $\mathrm{Im}(\epsilon_i^{-1})=-(\pi/2)\omega_{pi}\delta(\omega-\omega_{pi})$ for $i=1,2$, one sees from Eq. (3) that the sum over the surface terms is given by the same analytical function as the sum of the total corrections to the bulk loss probability in both media when both $\omega_{p1},\omega_{p2}\rightarrow\omega_m$. This property of the begrenzung has been found in other systems as well.[37,38,44,45] The function $\mathrm{Im}[\gamma_m(q,\omega)]$ provides the full surface excitation spectrum for a target of a given radius. The strength of each mode would depend on the electric field which excites the wire. To illustrate the previous formulation, we study the case of a metallic cylinder surrounded by vacuum. For the sake of simplicity, we use a real Drude dielectric function $\epsilon(\omega)=1-\omega_p^2/\omega^2$, where ω_p is the bulk-plasmon energy. In Fig. 1 we plot the imaginary part of the response functions $\mathrm{Im}[\gamma_m(q,\omega)]$ corresponding to $m=0$ and $m=1$ for Al ($\omega_p=15$ eV). The plots reproduce the dispersion relation as shown in Ref. 19 with the height derived from expression (7). Here we see that the excitation spectrum corresponding to $m=0$ contains all the energies below the planar surface plasmon $\omega_s=\omega_p/\sqrt{2}$, a limit value reached when $qa\gg1$. In the opposite limit, $q\rightarrow0$, the plasmon energy goes to zero, and consequently, the function $\mathrm{Im}[\gamma_m(q,\omega)]$ vanishes [Eq. (7)]. The plot corresponding to $m=1$ exhibits a weak dependence on q; this plot is indeed quite similar to the planar response function $\mathrm{Im}\{2/\epsilon_+1\}$, featuring a peak near ω_s. For $m>1$, the remaining response functions are very similar to this last case, featuring an even weaker dispersion. A simple case is that of the electron moving parallel to the axis of the target;[12] then the only contri-

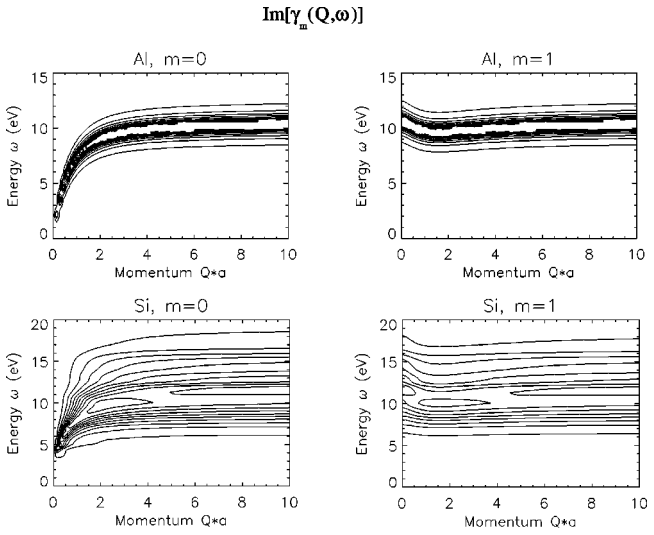

FIG. 1. Contour plots of the imaginary part of the cylindrical response functions $\gamma_m(q,\omega)$ [Eq. (4)] for $m=0$ and $m=1$, corresponding to Al and Si cylinders. For the Al cylinder, a Drude dielectric function has been used ($\omega_p=15$ eV). A small damping ($\gamma=1.06$ eV) has been considered in the dielectric function, $\epsilon(\omega)=1-\omega_p^2/\omega(\omega+i\gamma)$. Experimental optical data have been used for Si.

bution of the m mode to a given energy ω_m comes from $q=\omega_m v^{-1}$, where q is the solution of the dispersion equation $\omega_m^2=\omega_p^2(qa)I_m'(qa)K_m(qa)$.

In the lower side of Fig. 1, we represent the response functions $\mathrm{Im}[\gamma_m(q,\omega)]$ corresponding to a Si cylinder for $m=0$ and $m=1$. Here, due to the presence of a gap in the bulk response function, there is no excitation below $\omega=4.5$ eV. For $m=0$ and for small values of qa the loss peak is centered around 4.5 eV, and it exhibits a weak dependence on momentum q. For large values of qa the peak moves towards the value $\omega=10.3$ eV which roughly corresponds to the Si planar plasmon energy. As pointed out in the former case, the shape of this plot does not differ significantly from the planar response for $m>1$.

Now, we apply Eq. (3) to study the dependence of the strength of the surface excitations in a metallic wire as a function of the radius of the cylinder, for trajectories perpendicular to the axis, impact parameter $s=0$. Figure 2 shows the bulk correction (begrenzung) and the total probability of exciting surface plasmons as a function of the reduced diameter of the cylinder, $t=2a\omega v^{-1}$ ($\omega=\omega_p$ for the bulk correction curve and $\omega=\omega_s$ for the surface terms). The results are similar to those found for films and spheres:[43,45,46] the bulk correction goes to the thick film limit $\pi/2v$ for large values of t. Given that the direct bulk term depends linearly on t, this limiting value indicates that the begrenzung correction is relevant only for very thin targets ($a<v/\omega_p$). In the limit of very thin cylinders ($t\to 0$), this correction behaves like $t\ln(t)$ (i.e., it features the same dependence that has been found in films and spheres[43,46]). As pointed out by Ritchie,[43] this negative correction becomes larger than the direct bulk term for values of $2a<1/q_{max}$; this value imposes an obvious limit to the radius a for which the local dielectric approach is appropriate.

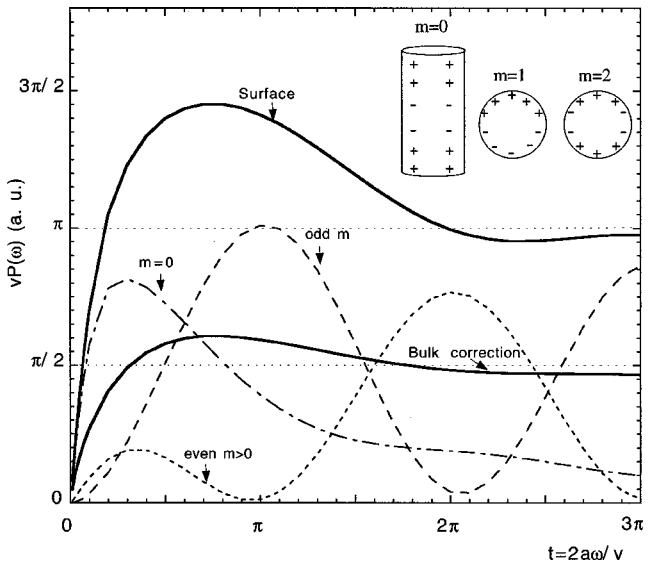

FIG. 2. Surface energy-loss probability and correction to the bulk energy-loss probability (*begrenzung* term) as a function of the reduced diameter $2a\omega v^{-1}$ for an electron moving perpendicularly to a metallic (Al) cylinder and passing by its axis ($s=0$). The frequency ω is ω_p for the bulk correction curve and $\omega_p/\sqrt{2}$ for the surface ones. The sums of even (short-dashed) and odd (long-dashed) multipolar terms have been distinguished in the surface probability. The contribution of the $m=0$ term is represented with dash-dotted line. The sign of the bulk correction term has been changed in order to fit it into the plot.

On the other hand, the total surface loss probability exhibits a more complex behavior. For very thin cylinders, the main contribution to the surface losses comes from the $m=0$ term. In the limit of very thin cylinders ($a\to 0$), the total probability of exciting surface plasmons can be written as follows:

$$P_{surf}=\frac{\pi}{v^2}\int_0^\infty dq\frac{\omega_0(qa)}{q^2+\dfrac{\omega_0(qa)^2}{v^2}}\frac{I_0(qa)}{K_0(qa)}, \tag{9}$$

where $\omega_0(qa)=\omega_p\sqrt{qaI_0'(qa)K_0(qa)}$ is the energy of the $m=0$ mode. In Eq. (9) the main contribution to the integral arises from small values of q, which correspond to an induced-charge density almost uniformly distributed across the cylinder surface; this is a mode which has a somehow monopolar character. In cylinders of finite length, such an extended excitation should be sensitive to the size of the cylinder and to the position of the beam relative to the edge of the wire; in this case, such a monopolar excitation has no physical meaning. We will study this effect in Sec. IV.

As shown in Fig. 2, the total probability of exciting surface plasmons approaches the thick film limit π/v when $t\gg 1$. An intuitive way of understanding the mechanism of excitation of surface plasmons and its geometrical dependence is provided by the analysis of the contribution of both even and odd modes to the total EELS. Similar to what happens in other kinds of targets,[47] this figure shows the presence of oscillations with maxima near $2a\omega_s v^{-1}=2\pi n$ (n

integer) for even m, and $2a\omega_s v^{-1}=2\pi(n+1/2)$ for odd m. A simple explanation for this derives from the fact that the azimuthal charge density of the mth modes goes as $\cos(m\phi)$; then, the charge distributions that the electron finds at the entrance and exit surface points of the cylinder are in phase (or out of phase) depending on whether the time spent by the electron to cross the cylinder $(2a/v)$ is an integer (or half an integer) times the plasmon period $2\pi/\omega_m(q)$, and consequently, it excites even (or odd) modes. The fact that all the $m>0$ modes $\omega_m(q)$ are very close to ω_s (Ref. 19) justifies that the maxima and minima occur at the same value of t. This plot means that for very thin wires the mode $m=2$ is stronger than the mode $m=1$. In general, the number of multipolar m terms involved in the spectra depends on the wire radius, impact parameter, and velocity of the probe: for penetrating trajectories and small values of t, few terms are needed, while for values of t larger than 1, many m terms are required to get good convergence (in Fig. 2 we have calculated up to $m=36$). We want to stress the fact that, although these curves have been obtained for a medium characterized by a Drude dielectric function, Fig. 2 is relevant to understanding the contributions to the energy loss in any medium. Figure 1 proves that only the energy of the $m=0$ mode differs significantly from the planar plasmon ω_s, and this plot shows that this mode dominates the spectrum for thin wires up to $a\sim v\,\omega_s^{-1}$; for larger values of the radius this mode vanishes and the spectrum does not differ from that corresponding to a film of the same thickness.

III. RESULTS FOR Si NANOWIRES

In this section, we study the case of Si cylinders in vacuum. The dielectric function $\epsilon(\omega)$ for crystalline Si used to reproduce the experimental results has been taken from Ref. 48.

We consider the surface energy-loss probability for a 100-keV electron crossing perpendicularly, i.e., at impact parameter $s=0$, the axis of a Si infinite cylinder of radius $a=2$ nm. To analyze the contributions of different values of q to the loss spectra, we write the surface contribution to the energy-loss probability (Eq. 3) as $P(\omega)=\Sigma_m\int dq\, P_m(q,\omega)$, where $P_m(q,\omega)$ provides the contribution to the total loss spectra of both q and m. In Fig. 3 we represent this function versus qa and ω. The sum over the first terms ($m=0,\ldots,4$) has been proven to be enough to get good convergence. The main features of this spectrum are a broad peak centered in energy $\omega=4.5$ eV and momentum $qa=0.13$, i.e., $q=1.6\omega/v=0.003$ a.u. and a negative peak which is the contribution of the begrenzung effect around the bulk-plasmon energy $\omega=16.7$ eV. Note that this second negative peak is more extended in the momentum scale. On the other hand, the first peak goes to zero as q tends to zero, but this is not the case of the second peak, which becomes positive in this limit. In Fig. 4(a) the surface contribution to the energy-loss probability has been plotted for an electron crossing perpendicularly the axis of a Si infinite cylinder of radius $a=2$ nm, at impact parameter $s=0$. The contribution of the first $m=0,1,\ldots,4$ terms has been considered in the summation. Although not strictly necessary from the mathematical point of view, to make the calculations of the surface contribution (3) consistent with the bulk term [Eq. (6)], we have used the same cutoff momentum for the integration, quoted as $q_{max}=0.3$ a.u. This value has been estimated by considering the minimum half wavelength associated with the charge oscillations, of the order of the lattice parameter of Si, $d=0.54$ nm, taken from the literature.[49] The surface contribution does not depend noticeably on this cutoff, as it will be justified further in this work. The first relevant point on this figure is the negative probability for energies around the Si bulk plasmon, centered at about 16.7 eV. This is the previously introduced begrenzung effect. All the multipolar terms contribute to the begrenzung but it mainly derives from the $m=0$ term. There are two surface peaks at 4.5 and 10.3 eV, which can be roughly associated to $m=0$ and $m\neq 0$, respectively. The $m=0$ mode provides the main surface contribution to the loss spectrum. Another relevant point is the higher contributions to the surface probability of even terms in relation to smaller-m odd terms. The explanation for this can be found in Fig. 2, since in our conditions, for the $m\neq 0$ surface-plasmon mode and for the radius considered, the reduced diameter t is about 0.42, around $\pi/10$, very close to the origin in Fig. 2. Note that in that region the dashed line corresponding to the even-modes contribution is above the odd-mode short-dashed line. The crossover would take place at about $t=0.25\pi$, corresponding to a wire radius of about 3.7 nm. In Fig. 4(b) we represent total-energy-loss spectra, i.e., taking into account the bulk contribution of Eq. (6). Now, in addition to the two surface peaks, the bulk peak around 16.7 eV appears. In this plot, contributions of small- and large-q values to the surface contribution have been singled out, showing a close relation between smaller values of q and the $m=0$ mode, a result which proves the extended charge-density pattern characteristic of this peak. The relative strength of these peaks depends on the impact parameter, and in this theoretical approach on the cutoff applied, but,

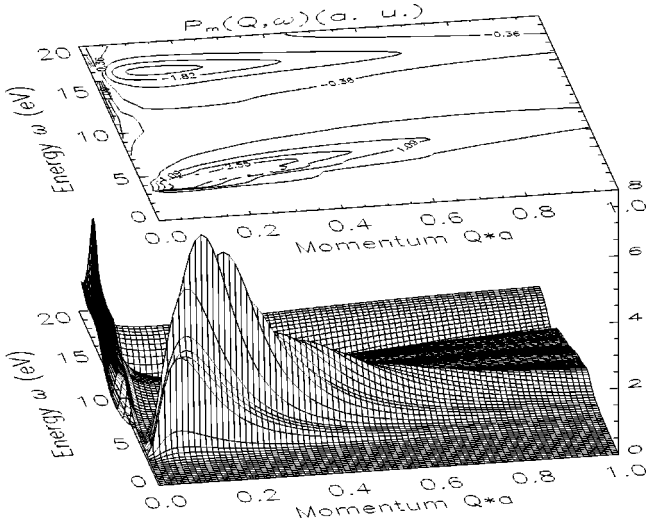

FIG. 3. Probability of transferring momentum q and energy ω, $P_m(q,\omega)$, to a Si wire of radius $a=2$ nm by a 100-keV electron crossing it perpendicularly and passing by its axis ($s=0$). The momentum q is scaled as qa. Contour plots have been added in the upper side.

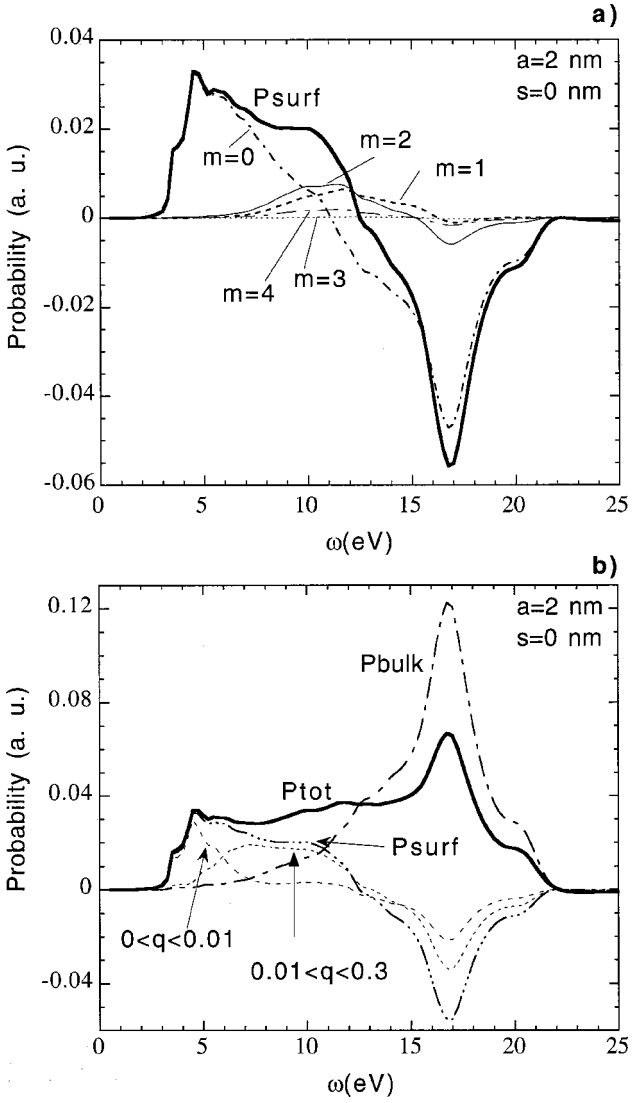

FIG. 4. (a) Surface and (b) total-energy-loss probability for 100-keV electrons crossing perpendicularly (impact parameter $s=0$) the axis of a Si nanowire of radius $a=2$ nm. In (a) the contributions of the $m=0$, 1, 2, 3, and 4 terms have been plotted as separate curves. In (b) the contributions of surface and bulk terms have been plotted separately. For the surface term, the partial contributions from two different q momentum intervals to the integral of Eq. (3) (namely, [0, 0.01] a.u. and [0.01, 0.3] a.u., respectively) have been singled out.

considering the broadness of the beam, one could conclude that the theoretical spectra present a good qualitative agreement with the experiment by Reed *et al.*[23] Both surface peaks have been found in EELS experiments near Si tips and filaments.[23] The peak of 4.5 eV was only measured for very small wires, as is the case considered in this plot. It is important for wire radii up to about 5 nm, whereas for thicker wires the spectra are dominated by the 10.3-eV peak, as can be deduced from Fig. 2. The second peak is the surface plasmon due to the $m\neq 0$ terms and it appears for all size wires. The redshift observed for this peak for wide filaments and distant trajectories has been attributed to retardation effects.[23] For penetrating trajectories passing close to the axis of the cylinder, the bulk excitation at 16.7 eV is the most important one for wires larger than $a=2$ nm.

The evolution of the three peaks with impact parameter s is studied in Fig. 5 for a silicon wire of 2-nm radius. Note that for external trajectories ($s>a$) the bulk contributions disappear and only the two surface peaks at 4.6 and 10.3 eV are present at the spectrum. The energies of the curves correspond to the positions of the peaks in Fig. 4. Note the sharp variation of the bulk peak ($\omega=16.7$ eV), whose probability falls nearly to zero at the cylindrical interface. The remaining tail for external trajectories is caused by the width of the surface peak. The surface-plasmon peak at 10.3 eV is maximum at the interface, decreasing more slowly inside than outside the cylinder.

Perhaps, the most relevant point from this figure is the rather flat curve corresponding to the low-energy peak ($\omega=4.5$ eV) which extends quite far away from the wire. This weak dependence on impact parameter has been experimentally found.[23] The slow change of the intensity of this peak with impact parameter is due to the fact that this mode corresponds to an azimuthally uniform induced-charge density on the surface and then it is only sensitive to an average value of the field; for thin wires the distance range of variation of the electric field produced by the probe is v/ω, about 20 nm for $\omega=4.5$ eV, much larger than the wire diameter, then the probability hardly changes with the variations of the impact parameter considered in this plot. This behavior is not present in EELS in other targets, such as clusters, where the surface peaks present an enhancement near the surface as the 10.3-eV peak. At large impact parameters, on the other side, this peak is the dominant one in the spectrum, as one would expect from the asymptotic behavior of the probability with distance; $P(\omega)$ behaves as $\exp(-2s\omega/v)$.[47] When the probe electrons travel parallel to the wire only excitations with momentum $q=\omega_m/v$ contribute to the m multipolar term of the loss probability. This is not the case for the perpendicular trajectory, when there is a range of q values contributing to the integral. In Fig. 6 we have plotted the relative weight of the different values of the upper limit q_{max} of the integral. The maximum value of q considered is 0.3 a.u., as argued in the beginning of this discussion. We have plotted two curves, corresponding to the peaks of 4.5 eV and 10.3 eV. Here we see that the contribution of high-q momenta is negligible for these excitations, and the q_{max} used is justified.

This particular spectrum of excitations, where the more relevant contribution comes from small values of q and low m, is hardly sensitive to the discrete radial structure of the electronic states of the wire, and therefore the use of dielectric theory properly describes the excitations of the wire. Note that the suitability of this approach cannot be extended as a general result for one-dimensional systems, even when considering the same target: it is limited to trajectories which excite very weakly the high azimuthal modes $m>0$. Furthermore, for penetrating trajectories as those studied here, the probability of exciting azimuthal modes strongly depends on the velocity of the probe through the parameter $a\omega v^{-1}$, as shown in Fig. 2, and therefore the faster the probe travels, the more suitable the dielectric response. A simple analysis of quantum confinement effects in thin cylinders[50] leads to a

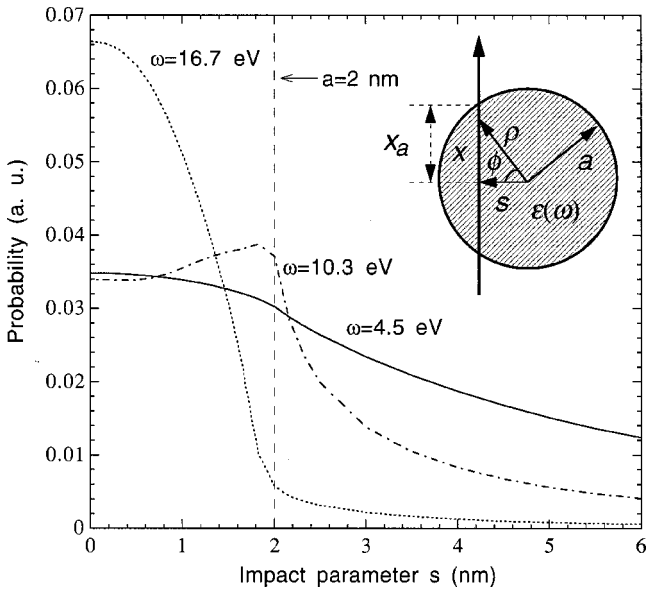

FIG. 5. Total-energy-loss probability as a function of impact parameter s, for 100-keV electrons crossing perpendicularly an $a=2$-nm-radius Si wire. The different lines correspond to loss probabilities at energies $\omega=4.5$, 10.3, and 16.7 eV.

rough estimation of the separation between energy subbands ΔE which scales as

$$\frac{\Delta E}{E}=\frac{R_0^2}{a^2}, \quad R_0=\sqrt{\frac{2\sqrt{2}\epsilon}{\omega_p m^*}}, \tag{10}$$

where E is the characteristic energy of the electronic states, ω_p the bulk-plasmon frequency of the wire material, ϵ its static dielectric constant, and m^* its effective mass. For Si this leads to $R_0 \sim 1$ nm, therefore this value states a lower limit to the applicability of the dielectric function in EELS analysis when radial excitations $m>0$ are dominant in the spectrum. One case which is likely to be out of the applicability limit should be that of an electron moving close and parallel to the surface of a thin nanowire; then, the surface response should contain high multipolar terms, and therefore it would fail to reproduce the real excitations. This discussion can be presumably applicable to the case of multishell fullerenes, where the coupling between inner and outer surfaces is weak. In the case of single-layer fullerenes, this coupling would induce a strong radial charge density and therefore it would be out of the limits of applicability of the dielectric response.

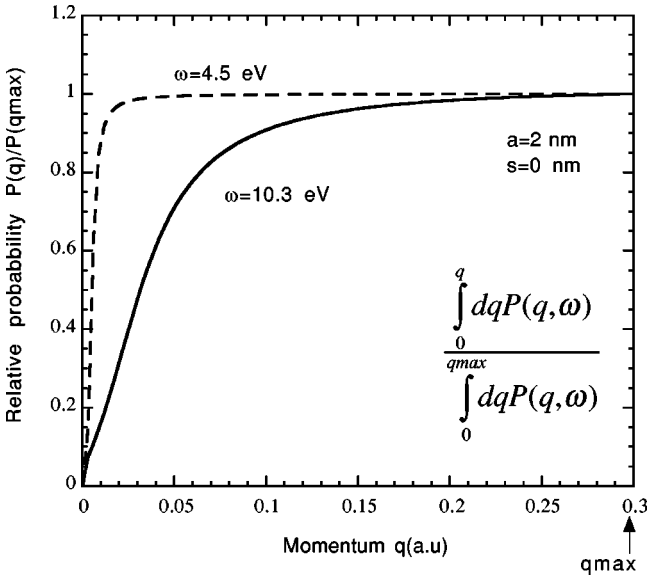

FIG. 6. Ratio of the total-energy-loss probability as a function of the maximum momentum q considered in the integration of Eq. (3), for the two peaks at $\omega=4.5$ eV and 10.3 eV. The maximum value of q considered in the integrations is 0.3 a.u.

This observation helps also to understand the insensitivity of the EELS technique to the real shape of the surface. The Si wire in the experiment we are analyzing presents many planar facets. The fact that the main excitation is longitudinal supposes that a fine description of the shape of the target is almost irrelevant. This is another way to look at a well-known result in EELS in STEM: the spatial resolution of this technique is v/ω, a length much larger in our case than the surface details to investigate.

Recently, Sander *et al.*[51] have reported EELS measurements in Bi wires, with radii in the range 35–90 nm, showing a clear redshift in the bulk-plasmon energy as the radius of the wire decreases. The authors suggest that this may be due to quantum confinement of the electronic states of the target, and the low effective mass of Bi supports that idea. Nevertheless, our preliminary calculations point out that this redshift may be also derived from the effect of the bulk-plasmon dispersion on the dielectric response of the medium: the larger the cylinder radius, the larger the weight of the small transversal component of the momentum in the dielectric function, and therefore, the smaller the dispersion effects. Furthermore, the redshift is observed in the experiments for electron beams passing by the center of the nanowires and in that situation only longitudinal excitations are produced ($m=0$), for which quantum confinement effects should be reduced, since the charge-density fluctuations extend primarily along the wire, that is, along the direction where quantum confinement is not taking place.

IV. EELS IN WIRES OF FINITE LENGTH

The target used in the experiments described in Ref. 23 consists of a very large (a few μm long) needle. Near the tip, the wire is almost cylindrical with a radius of about 2 nm. Up to now we have modeled the target as an infinite cylinder. The finite length of the wire poses two problems in relation to the former discussion: the first one is the energy of the surface modes corresponding to excitations localized near the tip and the second one is the influence of the beam position relative to the edge. The boundary charge method[34] (BCM) provides us with a useful tool for computing the energy loss spectra near targets of any complex geometry. It is based on the self-consistent calculation of the induced surface charge density to obtain the response of the target. We use this method to study the edge effects by modeling the target in the simplest way, as a semi-infinite cylinder closed

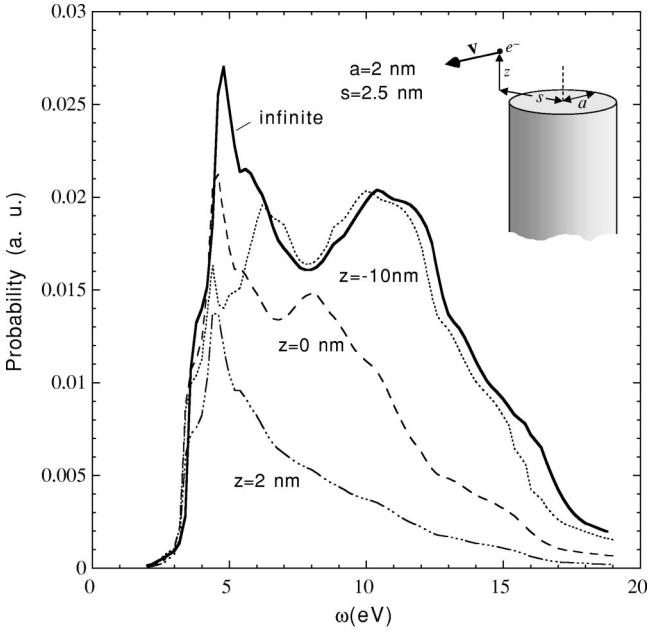

FIG. 7. EELS probability for 100-keV electrons traveling near a semi-infinite Si wire of radius $a=2$ nm, perpendicularly to the axis, at impact parameter $s=2.5$ nm and at different z distances from the edge (see inset).

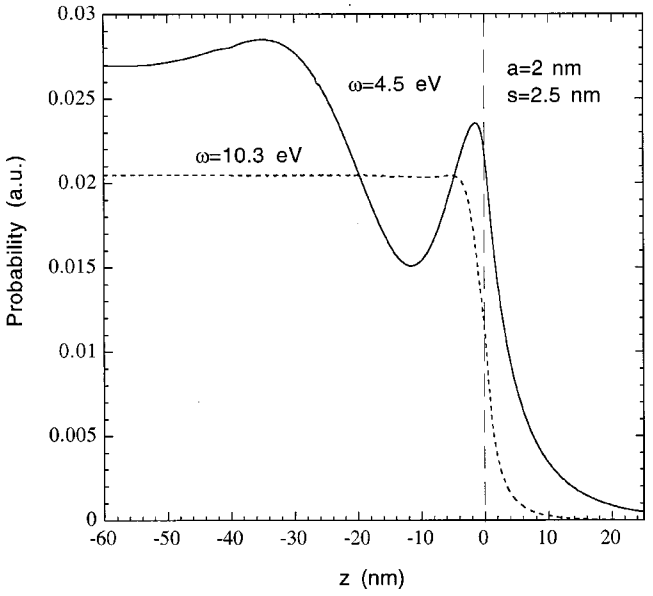

FIG. 8. EELS probability corresponding to the peaks at 4.5 eV and 10.3 eV in Fig. 7, as a function of the electron distance to the edge z, for a 100-keV electron moving perpendicularly to a Si wire of radius $a=2$ nm, at $s=2.5$ nm from its axis (see inset in Fig. 7).

by an abrupt planar cap. For wires of the size considered in this work, the surface of that cap is very small, so that the effect of this part of the induced charge on the spectra should be irrelevant unless the trajectory is very close to the edge. This means that the effect of the finite size of the wire can be studied without paying much attention to the specific shape of the boundary.

In Fig. 7 we plot the energy-loss probability corresponding to four different z beam positions, relative to the tip; positive values of z stand for probe trajectories in the far region with respect to the wire, while negative ones correspond to trajectories closer to the wire. The radius of the cylinder has been taken as $a=2$ nm and the radial impact parameter is $s=2.5$ nm in all cases (i.e., nonpenetrating trajectories are considered). All the spectra contain the sharp peak at 4.5 eV, which is the one corresponding to the $m=0$ mode. This result is in agreement with the findings of Ref. 23. Although for trajectories away from the edge ($|z|>v\omega^{-1}$) the $\omega=4.5$ eV peak is the main feature of the spectrum, it should be noted that the modes associated with the edge become the most relevant ones for smaller values of z. Some broad structures are found above the lower peak, but the spectrum corresponding to the infinite cylinder is recovered for large negative values of z. For beam trajectories away from the wire ($z=2$ nm) there is just one peak in the spectrum at 4.5 eV, a result showing that these excitations correspond to longitudinal fluctuations of the induced surface charge density along the cylinder. As the probe travels closer to the tip, some peaks show up in the $7-10$-eV region, which are related to the modes of the edge and are sensitive to the kind of surface chosen to close the cylinder. Similar excitations have been observed in Si-SiO_2 I-type junctions.[52] Note that for $z=-10$ nm the peak at 10.3 eV is almost identical to that of the infinite cylinder, while the intensities of the low-energy $m=0$ peaks are quite different. In this figure it can also be noticed that the 4.5-eV peak does not increase monotonously as the probe is moved far away from the edge, but it has an oscillatory behavior.

The evolution of the intensity of both of these peaks towards their infinite cylinder values is shown in Fig. 8 as a function of distance z (see the inset in Fig. 7). The 10.3-eV probability increases rapidly near the edge and stabilizes soon, reaching the value of the infinite wire, while the low-energy peak ($\omega=4.5$ eV) exhibits strong intensity modulations. This behavior can be explained by considering the mean values of the longitudinal momentum q involved in each of these two excitation energies for the infinite cylinder calculations. For $\omega=10.3$ eV and a radius $a=2$ nm, the mean momentum involved in the integration is about 0.04 a.u. (see Fig. 3), and thus, its associated wavelength is of the order of 8 nm, a value close to the range of the corresponding ω component of the external field created by the electron, v/ω. This means that the effect of the edge is governed by the range of the external electron potential in this case, where $m>1$ modes are dominating. Quite differently, the mean q value for the $\omega=4.5$-eV excitation (which is primarily connected to the excitation of $m=0$ modes) is about 0.005 a.u., and therefore, its associated range is of the order of 50 nm, so that the infinite wire limit is reached for large values of $-z$, far away from the wire edge. In brief, this latter behavior is attributed to the momentum q of the longitudinal excitations involved in the infinite wire, which is smaller in the low-energy peak, and therefore this peak is more sensitive to the tip position up to a distance of the order of the wavelength of the corresponding charge-density fluctuations. This simple argument permits to explain qualitatively the behavior of the two curves shown in Fig. 8. Notice that $m>0$

modes have regions with opposite sign of the induced charge that are closer together as compared with the $m=0$ modes (see the insets in Fig. 2). Therefore, the interaction among the induced charge in $m=0$ modes can play a role at larger distances, and this provides another intuitive argument for the behavior discussed in the last paragraph.

In Fig. 8, the probability corresponding to the modes associated to the edge are not included because they would depend on the surface used to close the tip. Nevertheless, the minimum exhibited by the 4.5-eV peak in this figure can be interpreted as a consequence of the sum rules of the surface-plasmon modes:[53] the excitation of edge-related modes occurs at the expense of the other surface modes. Moreover, for trajectories away from the tip ($z>0$) the intensity of these modes decays with the general impact-parameter dependence found in EELS, $P(\omega)=\exp(-2z\omega/v)$, and therefore, only the $m=0$ is effectively excited at large impact parameters.

V. CONCLUSIONS

EELS spectra obtained for electrons traveling perpendicularly to thin wires of a few nm in radius have been studied within the frame of classical dielectric theory, first by modeling the nanowires as infinite cylinders and later by considering edge effects using the BCM method. The general dependence of both surface- and bulk-plasmon excitations on the size of the target has been analyzed for metallic Drude wires and compared with results obtained for spherical particles and thin films, finding a similar dependence with the length of the electron path inside the target.

Our calculations have been compared with experiments performed in silicon filaments, describing both the origin and spatial extension of the low-energy-loss peak (at 4.5 eV), which has been associated with longitudinal charge oscillations of monopolar character ($m=0$), and the other surface-plasmon excitations at about 10.3 eV, associated with multipolar $m>0$ excitations. The impact-parameter-dependence study has revealed the predominance of the 4.5-eV energy peak for very thin (radius $a=2$ nm) wires. Dielectric response theory has demonstrated to be valid for wires of radii down to 2 nm. The spatial extension of the effect of the edge for terminated wires (i.e., the range of distances to the edge for which the infinite wire approximation is valid) has been evaluated for losses of 4.5 eV and 10.3 eV, respectively, and justified in terms of the value of the momenta q that are contributing significantly to the energy-loss probability.

ACKNOWLEDGMENTS

The authors wish to thank Professor P. M. Echenique and I. Juaristi for many stimulating suggestions and help. Support from the Basque government and Basque Country University is acknowledged. One of the authors (E.O.) also acknowledges the Spanish Ministerio de Educación y Cultura for financial support under Contract No. PB98-0780-C02.

[1] S. Ijima, Nature (London) **354**, 56 (1991).
[2] M.S. Dresselhaus, G. Dresselhaus, and P. C. Eklund, *Science of Fullerenes and Carbon Nanotubes* (Academic Press, San Diego, 1996).
[3] S. Seraphin, D. Zhou, J. Jiao, J.C. Withers, and R. Loutfy, Nature (London) **362**, 503 (1993).
[4] D. Ugarte, T. Stöckli, J.M. Bonard, A. Chatelain, and W.A. De Heer, Appl. Phys. A: Mater. Sci. Process. **A66**, 1 (1998).
[5] Y. Zhang, K. Suenaga, C. Colliex, and S. Ijima, Science **281**, 973 (1998).
[6] T. Pichler, M. Knupfer, M.S. Golden, and J. Fink, Phys. Rev. Lett. **80**, 4729 (1998).
[7] R. Kuzuo, M. Terauchi, and M. Tanaka, Jpn. J. Appl. Phys., Part 2 **31**, L1484 (1992).
[8] T. Stöckli, Z.L. Wang, and A. Chatelain, Philos. Mag. B **79**, 1531 (1999).
[9] K. Suenaga, C. Colliex, N. Demoncy, A. Loiseau, H. Pascard, and F. Willaime, Science **278**, 653 (1997).
[10] C. Miziumski, Phys. Lett. **40A**, 187 (1972).
[11] J.C. Ashley and L.C. Emerson, Surf. Sci. **41**, 615 (1974).
[12] Y.T. Chu, R.J. Warmack, R.H. Ritchie, W. Little, R.S. Becker, and T.L. Ferrell, Part. Accel. **16**, 13 (1984).
[13] C.A. Walsh, Philos. Mag. A **59**, 227 (1989).
[14] A. Howie and C.A. Walsh, Microsc. Microanal. Microstruct. **2**, 171 (1991).
[15] N. Zabala, A. Rivacoba, and P.M. Echenique, Surf. Sci. **209**, 465 (1989).
[16] M.F. Lin and K.W.W. Shung, Phys. Rev. B **50**, 17 744 (1994).
[17] M.F. Lin, D.S. Chuu, C.S. Huang, Y.K. Lin, and K.W.W. Shung, Phys. Rev. B **53**, 15 493 (1996).
[18] P. Apell and G. Mukhopadhyay, Solid State Phys. **35C**, 397 (1992).
[19] A. Rivacoba, P. Apell, and N. Zabala, Nucl. Instrum. Methods Phys. Res. B **96**, 465 (1995).
[20] G.F. Bertsch, H. Esbensen, and B.W. Reed, Phys. Rev. B **58**, 14 031 (1998).
[21] A.A. Lucas, L. Henrard, and Ph. Lambin, Phys. Rev. B **49**, 2888 (1994).
[22] J.M. Pitarke and A. Rivacoba, Surf. Sci. **377-379**, 294 (1997).
[23] B.W. Reed, J.M. Chen, N.C. MacDonald, J. Silcox, and G.F. Bertsch, Phys. Rev. B **60**, 5641 (1999).
[24] F. Ouyang, P.E. Batson, and M. Isaacson, Phys. Rev. B **46**, 15 421 (1992).
[25] J. Aizpurua, A. Rivacoba, and P. Apell, Phys. Rev. B **54**, 2901 (1996).
[26] R.P. Fehlhaber and L.A. Bursill, Phys. Rev. B **60**, 14 147 (1999).
[27] R.P. Fehlhaber and L.A. Bursill, Phys. Rev. B **62**, 17 094 (2000).
[28] C. Bréchignac, Ph. Cahuzac, L. Leygnier, and A. Sarfati, Phys. Rev. Lett. **70**, 2036 (1993).
[29] T. Reiners, C. Ellert, M. Schmidt, and H. Naherland, Phys. Rev. Lett. **74**, 1558 (1995).
[30] N. Zabala, M.J. Puska, and R.M. Nieminen, Phys. Rev. Lett. **80**, 3336 (1998).
[31] N. Zabala, M.J. Puska, and R.M. Nieminen, Phys. Rev. B **59**, 12 652 (1999).

[32] J.C. Ashley and L.C. Emerson, Surf. Sci. **41**, 615 (1974).
[33] C.A. Pfeiffer, E.N. Economou, and K.L. Ngai, Phys. Rev. B **10**, 3038 (1974).
[34] F.J. García de Abajo and J. Aizpurua, Phys. Rev. B **56**, 15 873 (1997).
[35] F.J. García de Abajo and A. Howie, Phys. Rev. Lett. **80**, 5180 (1998).
[36] A. Rivacoba, N. Zabala, and P.M. Echenique, Phys. Rev. Lett. **69**, 3362 (1992).
[37] A. Howie and R.H. Milne, Ultramicroscopy **18**, 427 (1985).
[38] R. Nuñez, P.M. Echenique, and R.H. Ritchie, J. Phys. C **13**, 4229 (1980).
[39] P.M. Echenique, R.H. Ritchie, N. Barberán, and J. Inkson, Phys. Rev. B **23**, 6486 (1981).
[40] N. Zabala and P.M. Echenique, Ultramicroscopy **32**, 327 (1990).
[41] J. Aizpurua, Ph.D. thesis, University of the Basque Country, 1998; J. Aizpurua and E. Uranga, Scanning Microsc. **12**, 255 (1998).
[42] D. Pines and D. Bohm, Phys. Rev. **8**, 338 (1952).
[43] R.H. Ritchie, Phys. Rev. **106**, 874 (1957).
[44] M. Schmeits, J. Phys. C **14**, 1203 (1981).
[45] P.M. Echenique, J. Bausells, and A. Rivacoba, Phys. Rev. B **35**, 1521 (1987).
[46] A. Rivacoba and P.M. Echenique, Scanning Microsc. **4**, 73 (1990).
[47] A. Rivacoba, N. Zabala, and J. Aizpurua, Prog. Surf. Sci. **65**, 1 (2000).
[48] D.E. Aspnes and A.A. Studna, Phys. Rev. B **27**, 985 (1983). There are slight differences in the literature which affect the position of the bulk and planar surface plasmon but the low-energy region, $\omega < 6$ eV, is the same. Nevertheless, those differences do not change the discussion of this work.
[49] H. Ibach and Hans Lüth, *Solid-State Physics* (Springer, Berlin, 1991).
[50] C.R. Proetto, Phys. Rev. B **45**, 11 911 (1992).
[51] M.S. Sander, R. Gronsky, Y.M. Lin, and M.S. Dresselhaus, J. Appl. Phys. **89**, 2733 (2001).
[52] J. Aizpurua, A. Howie, and F.J. García de Abajo, Phys. Rev. B **60**, 11 149 (1999).
[53] S.P. Apell, P.M. Echenique, and R.H. Ritchie, Ultramicroscopy **65**, 53 (1996).